RESEARCH PAPER

PCCP www.rsc.org/pccp

Ti diffusion in La-doped $SrTiO_3$ single crystals†

Karsten Gömann,*[a] Günter Borchardt,[a] Anissa Gunhold,[b] Wolfgang Maus-Friedrichs[b] and Horst Baumann[c]

[a] *Institut für Metallurgie, Technische Universität Clausthal, Robert-Koch-Str. 42, D-38678 Clausthal-Zellerfeld, Germany. E-mail: karsten.goemann@tu-clausthal.de; Fax: +49 5323 72-3184; Tel: +49 5323 72-3688*

[b] *Institut für Physik und Physikalische Technologien, Technische Universität Clausthal, Germany*

[c] *Institut für Kernphysik, Universität Frankfurt, Germany*

Received 24th November 2003, Accepted 1st March 2004
First published as an Advance Article on the web

Titanium tracer diffusivities were determined in donor doped $SrTiO_3$ at temperatures between 1573 and 1673 K in synthetic air. La-doped $SrTiO_3$ single crystals cut in the three crystal orientations (100), (110), and (111), were used. After annealing, the well known formation of SrO islands is observed. Their number and size increase with the La content supporting the model that under oxidizing conditions the dopant is compensated by Sr vacancies. Tracer sources of ^{49}Ti or ^{50}Ti were applied by ion implantation. The resulting depth profiles were measured by secondary ion mass spectrometry (SIMS). The bulk Ti tracer diffusivity is found to be several orders of magnitude lower than the O diffusivity and also the La and Nd diffusivities reported recently. In contrast to La, the Ti tracer profile broadening shows largely ideal behaviour. As even long term annealing (several weeks) of weakly doped $SrTiO_3$ does not lead to significant tracer migration, the Ti diffusion seems to be enhanced by the presence of the donor induced Sr vacancies. Although microscopic investigations undertaken on the same samples show strong differences in the surface reconstruction depending on the crystal orientation, no orientation dependence of the Ti diffusivity is observed.

1 Introduction

Perovskites like strontium titanate $SrTiO_3$ are widely used electronic materials (see, *e.g.*[1]). Doping of $SrTiO_3$ with donor atoms like lanthanum or niobium yields a promising material for resistive high temperature oxygen sensors. Unfortunately, changing the surrounding oxygen partial pressure $p(O_2)$ at high temperature results in an unwanted surface reconstruction and secondary phase formation. The parameters influencing the surface reconstruction and phase formation are the temperature, the composition of the surrounding atmosphere, the crystal orientation and the dopant concentration.

Many of the observed phenomena can be explained by the defect chemistry model of donor doped $SrTiO_3$.[2] The bulk defect chemistry is governed by the following reaction (for defect notation see[3]):

$$V_O^{\cdot\cdot} + 2e' + \frac{1}{2}O_{2(g)} \Leftrightarrow O_O^{\times} \qquad (1)$$

Upon oxidation of O deficient strontium titanate, $V_O^{\cdot\cdot}$ and free electrons are consumed by the incorporation of O into the lattice. In return, cation vacancies are generated and a subsequent change in the donor compensation mechanism occurs. Although in principle both Sr and Ti vacancies may be generated, in the opinion of most authors the formation of $V_{Ti}^{''''}$ defects is unlikely not only because of the high relative charge. Electrical conductivity and gravimetrical measurements,[4,5] the amount of O uptake during the compensation change,[6] the formation of Sr vacancies in solid solutions of $SrTiO_3$ and $La_{2/3}TiO_3$,[7] experiments on the secondary phase formation on different $(Sr,La)TiO_3$ stoichiometries[8] and computer simulation studies[9] all argue for a compensation by Sr vacancies. Only one computer simulation study favours compensation by a complete Schottky reaction.[10]

The excess Sr may remain in the crystal forming layered Ruddlesden–Popper phases ($SrO{\cdot}nSrTiO_3$, [11]),[12,13] but yet no experimental evidence has been found for this assumption.[14] Certainly, excess Sr migrates to the surface where secondary SrO_x phases grow on top of the surface (*e.g.*[15–17]), and Ruddlesden–Popper phases are formed at the surface between the islands:[18,19]

$$Sr_{Sr}^{\times} + 2e' + \frac{1}{2}O_{2(g)} \Leftrightarrow V_{Sr}'' + SrO_{sec\text{-}phase} \qquad (2)$$

The amount of V_{Sr}'' produced is fixed by the donor content

$$[D^{\cdot}] = 2[V_{Sr}''] \qquad (3)$$

explaining the correlation of secondary phase quantity and dopant concentration. If the formation of strontium vacancies is thus restricted to the surface, then the rate-limiting step of the re-equilibration is the strontium diffusion and the strong differences in point defect mobility lead to a space charge zone in the near surface region.[14]

Upon reduction at low $p(O_2)$, the O_2 release into the atmosphere is accompanied by the generation of electrons, which partly reduce Ti^{4+}, resulting in the formation of Ti^{3+} containing phases like Ti_2O_3 or $LaTiO_3$.[20–22]

For a better understanding of the kinetics of these reactions, the mobilities of the involved species must be known. Meanwhile the depth-dependent O diffusion coefficient is well known and a Sr vacancy diffusion coefficient was deduced from it,[14,23] which is in acceptable agreement with a measured value.[24] Still, there exist only a few publications on cation diffusion: An experimental study on Sr and Ti diffusion in undoped $SrTiO_3$ at 2148 K, focussing on the dislocation dependence[25]

† Presented at the 85th Bunsen Colloquium on "Atomic Transport in Solids: Theory and Experiment", Gießen, Germany, October 31, 2003.

DOI: 10.1039/b315210c

and one computer simulation study.[9] Continuing our previous work on La and Nd diffusion in La-doped $SrTiO_3$,[26] we now will present results on Ti diffusion experiments under oxidizing conditions.

2 Experimental

2.1 Sample preparation

Commercial $SrTiO_3$ single crystals in the crystallographic orientations (100), (110), and (111) and with lanthanum contents of 0, 0.02, and 1 at% were obtained from Crystec (Berlin, Germany). As the crystals are grown under reducing conditions, the samples were equilibrated for 4–6 weeks at 1573 K and for 2 weeks at 1673 K, respectively. All annealings took place in an alumina tube furnace in a continuous flow of synthetic air (20% O_2, 80% N_2) at ambient pressure.

Within the first hours the annealing was interrupted several times to examine the secondary phase formation and surface reconstruction with spectroscopic and microscopic methods, including scanning electron, atomic force and scanning tunneling microscopy (SEM, AFM, STM), photoelectron, metastable impact and Auger electron spectroscopy (XPS, UPS, MIES, AES), and electron probe microanalysis (EPMA). The results are not included in this publication but partially already published elsewhere.[17,18,21,22,26–28]

As stated above, annealing of reduced $SrTiO_3$ under oxidizing conditions leads to the formation of strontium oxide islands on top of the surface. As the extent of formation increases with the donor dopant concentration, the observed coverages do not exceed 1% on the lower and undoped samples but reach up to 40% on the 1 at% La-doped samples. Typical micrographs of the surfaces after equilibration are shown in Fig. 1. The oriented growth of the secondary islands can clearly be seen. The islands have to be removed prior to tracer deposition in order to obtain pure $SrTiO_3$ bulk diffusion coefficients. Therefore, the 1 at% La-doped samples were washed for 24 h at 60 °C in deionized water, thus removing the secondary phases quantitatively from the (100) and (111) surfaces, where the SrO_x islands seem to grow flat on top of the surface. In contrast, on the (110) surfaces remnants of the islands with partly topographically negative features are observed (see Fig. 2), indicating that in this case the phases had grown partially downwards into the $SrTiO_3$ crystal.

2.2 Tracer ion implantation

$^{49}Ti^+$ or $^{50}Ti^+$ tracer ions were introduced into the sample *via* ion implantation using a mass separated and scanned beam with a dose of 1×10^{16} cm^{-2} at 50 keV and room temperature. After implantation, the tracer ions possess ideally a Gaussian distribution which can be expressed by the following formula:[29]

$$c(x,t) = \frac{N}{\sqrt{2\pi(\sigma^2)}} \exp\left(-\frac{(x-x_c)^2}{2\sigma^2}\right) \qquad (4)$$

with c being the concentration, x the depth, t the time, N the implanted fluence, σ the standard deviation of the distribution and x_c the mean value of the projected range.

Thermal treatment of the samples leads to diffusion of the tracer followed by a broadening of the Gaussian profile. The tracer diffusion coefficient D may then be derived directly from the increase in σ by fitting the adequate solution of

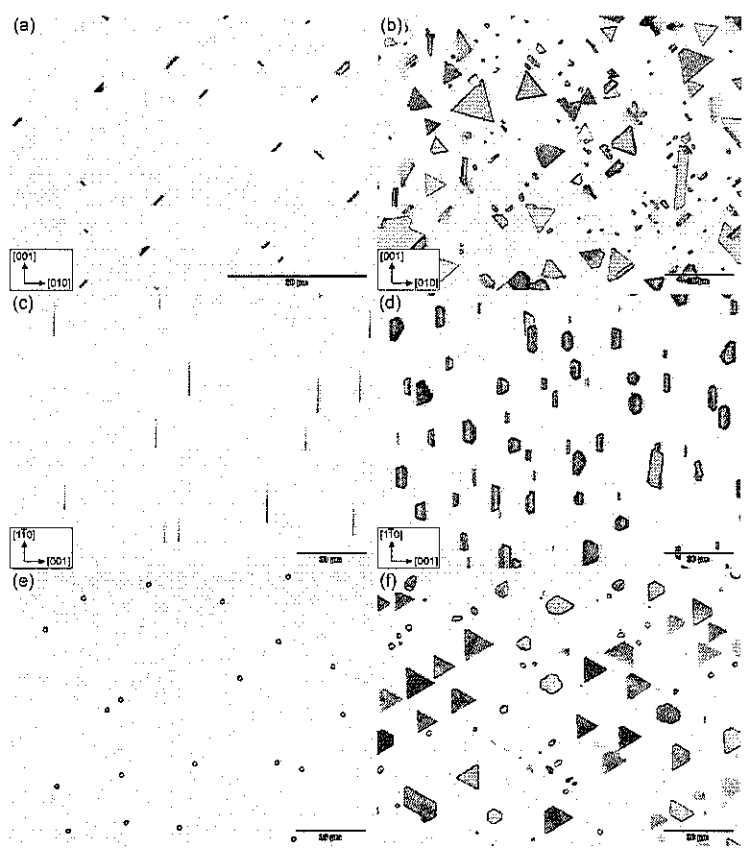

Fig. 1 Optical micrographs of $SrTiO_3$ surfaces after equilibration. (a) 0.02 at% La, (100) surface; (b) 1 at% La, (100) surface; (c) 0.02 at% La, (110) surface; (d) 1 at% La, (110) surface; (e) 0.02 at% La, (111) surface; (b) 1 at% La, (111) surface.

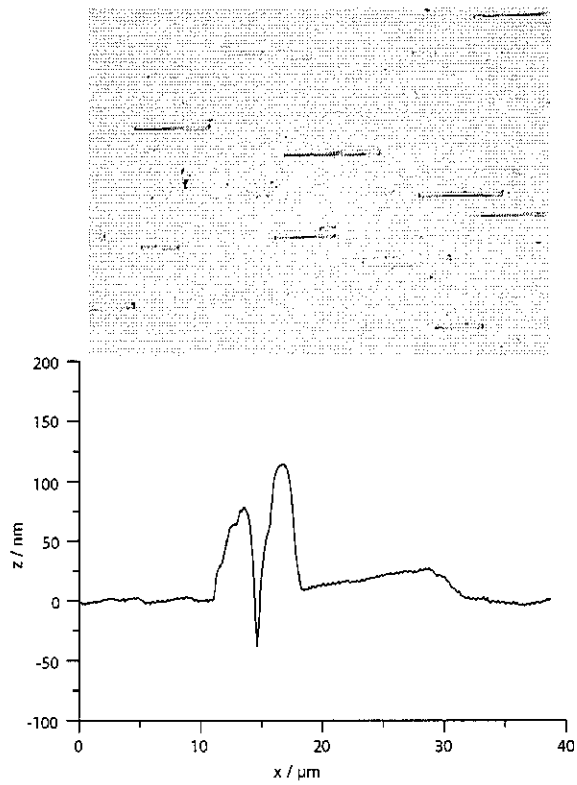

Fig. 2 Strontium oxide island residues after washing on a 1 at% La-doped $SrTiO_3(110)$ sample. Top: optical micrograph; bottom: surface profiler line scan across island residue.

Fick's second law to the measured depth profiles:

$$c(x,t) = \frac{N}{\sqrt{2\pi(\sigma^2 + 2Dt)}} \exp\left(-\frac{(x-x_c)^2}{2\sigma^2 + 4Dt}\right) \quad (5)$$

leads to:

$$D = \frac{\sigma_{post}^2 - \sigma_{pre}^2}{2t} \quad (6)$$

with σ_{pre} and σ_{post} being the σ values measured before and after the respective annealing step.

2.3 SIMS depth profile analysis

The depth distribution of all ions was measured by SIMS. Prior to analysis, all samples were coated with a carbon layer of 10 to 30 nm thickness to prevent charging. In contrast to gold coatings, the C layer is easily removed by oxidation to CO_2 at the beginning of the next annealing step, facilitating several consecutive experiments with each sample. Comparative measurements with 30 nm Au coating showed no significant difference in profile shape.

The majority of the measurements was performed with a Cameca IMS 3f using a 10 keV O^- primary ion beam and a primary current of 30 to 100 nA. An area with a diameter of about 60 μm in the center of the sputtered area of 250 × 250 μm^2 was gated for signal detection. For some measurements also a Cameca IMS 4f machine at CNRS Meudon-Bellevue (France) was used with a Cs^+ primary beam operated at 10 keV and 15 nA with a raster size of 125 × 125 μm^2, detecting secondary positive ions in conjunction with a normal incident electron gun. The results of these measurements do not differ significantly from the Clausthal measurements. The crater depths were measured using surface profilers (Tencor Alpha-Step500 and Tencor P-1).

Because of the long analysis duration, in general only one SIMS depth profile was recorded after each experiment, making a direct estimation of the analytical reproducibility difficult. But, as no diffusion was observed on the less and undoped samples (for discussion see Section 3.2), these measurements can conveniently be used to calculate an overall standard deviation s of the measured σ values including errors from the crater depth measurement and the fitting procedure after the following formula (see, *e.g.*,[30]):

$$s = \sqrt{\frac{\sum(\sigma_{i1} - \bar{\sigma}_1)^2 + \sum(\sigma_{i2} - \bar{\sigma}_2)^2 + \cdots + \sum(\sigma_{iN} - \bar{\sigma}_N)^2}{n_1 - 1 + n_2 - 1 + \cdots + n_N - 1}} \quad (7)$$

where σ_{i1} and σ_{iN} are single values of the first and the Nth sample, respectively. $\bar{\sigma}$ is the mean value, n the number of single values of the respective sample. From the data compiled in Table 1 a value of $s = 0.96$ nm is deduced. At high σ values after long annealing, the error of the Gaussian fit becomes larger than s. In these cases, the fit error was used for error bars.

3. Results and discussion

3.1 Depth profiles

Fig. 3 shows the raw data of a typical SIMS depth profile after subtraction of the conducting carbon layer. In this case, ^{49}Ti was implanted. At the surface enhanced Ti signals are observed accompanied by a reduced La signal, whereas the Sr signal remains constant. This behaviour is attributed to preferential sputtering, which is a common phenomenon in multicomponent systems, leading to an augmented sputtering of the lighter components at the beginning of the process.[31] For correction the measured tracer intensity was normalized to a second Ti isotope, which is assumed to be naturally distributed throughout the whole sample, hereby calculating the atomic fraction of the tracer isotope:

$$[^{49}Ti] = \frac{I(^{49}Ti)}{\frac{I(^{49}Ti)}{0.0541} + \left(I(^{50}Ti) - \frac{0.0518\,I(^{49}Ti)}{0.0541}\right)} \quad (8)$$

with I being the measured intensity and 0.0541 and 0.0518 the natural abundances of the isotopes ^{49}Ti and ^{50}Ti, respectively.

In Fig. 4 a typical sequence of depth profiles for a 1 at% La-doped sample is shown. A consecutive broadening of the Gaussian profile can be seen, following the behaviour described in eqn. (5). Earlier experiments on lanthanum

Table 1 σ values of the undoped and 0.02 at% La-doped samples. $\sigma(t)$: value measured after the respective annealing time t; $\bar{\sigma}$: average σ value

		$\sigma(t)$				
$t@T = 1573$ K	$\bar{\sigma}$	0.5 h	+4 h	+3 d	+28 d	+47 d
$SrTiO_3(110)$, undoped	22.3	23.3	23.4	21.2	21.7	21.8
$SrTiO_3(100)$, 0.02 at% La	20.7	20.8	20.5	20.8	20.7	—
$SrTiO_3(110)$, 0.02 at% La	20.4	20.9	21.0	20.6	19.1	—
$t@T = 1673$ K		0.25 h	+1 h	+24 h	+14 d	+27 d
$SrTiO_3(100)$, undoped	19.3	18.2[a]	19.9	18.2	20.9	—
$SrTiO_3(100)$, 0.02 at% La	22.0	21.0	23.2	23.8	19.7	22.3
$SrTiO_3(110)$, 0.02 at% La	23.0	23.0	24.0	22.3	21.9	23.9
$SrTiO_3(111)$, 0.02 at% La	21.6	20.7	22.2	22.4	21.2	—

[a] Value measured at $t = 0$.

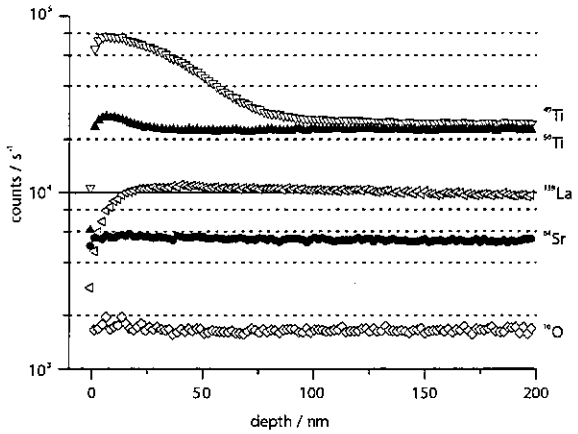

Fig. 3 Raw SIMS depth profile data of a 1 at% La-doped $SrTiO_3$(110) sample annealed for 1 h at 1673 K.

diffusion in the same material showed a distortion of the Gaussian tracer profiles at depths $< x_c$.[26] This distortion was attributed to radiation damage, which is introduced into the lattice during the implantation process. Though the same fluence was used during La implantation, the acceleration energy (120 compared to 50 keV) and the ion mass (139 compared to 49 or 50 u) were higher. For the above parameters and a density of 5.12 g cm^{-3}, the SRIM 2003 computer code ("stopping and range of ions in matter",[32]) calculates the generation of 678 vacancies/ion for ^{49}Ti implantation and 1703 vacancies/ion for ^{139}La implantation, indicating that the amount of radiation damage is substantially lower in the case of Ti.

3.2 Diffusion coefficients

As described in Section 2., Gaussian functions were fitted to the experimental data and D values were calculated from the change in width of the Gaussian profiles. The obtained values for the 1 at% La-doped samples are compiled in Table 2. Although surface reconstruction and island formation depend on the surface orientation (see above), the diffusion coefficients seem to be isotropic. This is in agreement with the results for lanthanum[26] and is expected for a cubic crystal.

The as-implanted profiles of all samples yield an average σ value of about 18 nm, which is larger than the value of 13.6 nm obtained from simulation with SRIM. This broadening is a typical result of ion beam mixing during the SIMS analysis and surface roughness. The correction procedure which

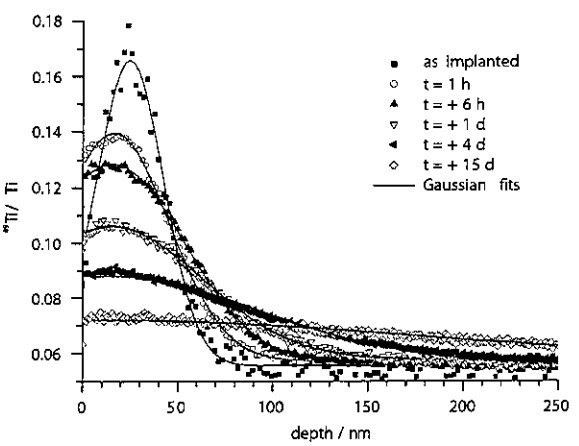

Fig. 4 ^{49}Ti depth profiles obtained with SIMS on a 1 at% La-doped $SrTiO_3$(110) sample with progressive annealing duration t at 1673 K.

Table 2 σ and D values of the 1 at% La-doped samples. t_{tot} – total annealing time; D – calculated from σ of the previous measurement and t; D_{tot} – calculated from the first σ value and t_{tot} (see eqn. 6)

Orientation	T/K	t/h	t_{tot}/h	σ/nm	D/m^2 s^{-1}	D_{tot}/m^2 s^{-1}
(100)	1573	0.5	0.5	21.0	—	—
		4	4	23.6	4.1×10^{-21}	4.1×10^{-21}
		72	76	28.5	4.9×10^{-22}	6.8×10^{-22}
		348	424	84.4	2.5×10^{-21}	2.2×10^{-21}
(100)	1673	0	0	17.1	—	—
		1	1	22.9	3.2×10^{-20}	3.2×10^{-20}
		24	25	52.3	1.3×10^{-20}	1.4×10^{-20}
		96	121	74.1	4.0×10^{-21}	$6.0 \times 10_{-21}$
		360	481	154	7.0×10^{-21}	6.7×10^{-21}
(110)	1673	0	0	17.8	—	—
		1	1	30.3	8.3×10^{-20}	8.3×10^{-20}
		6	7	38.5	1.3×10^{-20}	2.3×10^{-20}
		24	31	50.5	6.2×10^{-21}	1.0×10^{-20}
		96	127	80.8	5.8×10^{-21}	6.8×10^{-21}
		360	487	164	7.8×10^{-21}	7.5×10^{-21}
(111)	1673	0.25	0.25	25.0	—	—
		1	1	32.8	6.3×10^{-20}	6.3×10^{-20}
		24	25	51.8	9.3×10^{-21}	1.1×10^{-20}
		96	121	93.2	8.7×10^{-21}	9.3×10^{-21}
		360	481	223	1.6×10^{-20}	1.4×10^{-20}

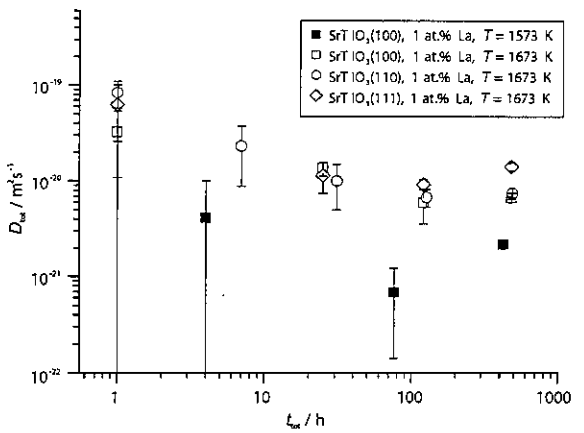

Fig. 5 D values of the 1 at% La-doped samples plotted against the annealing time. error bars are 2s values (for calculation see Section 2.3).

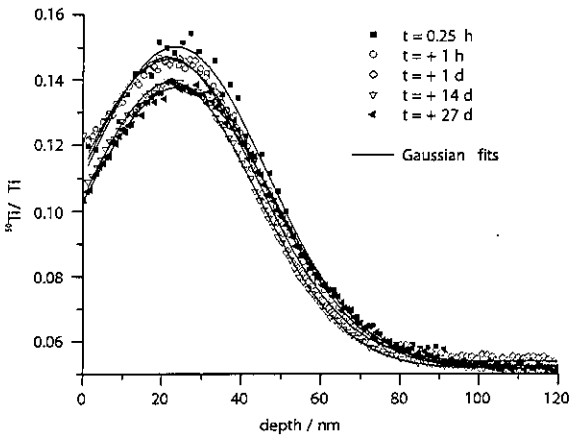

Fig. 6 ^{50}Ti depth profiles obtained with SIMS on a 0.02 at% La-doped $SrTiO_3$(110) sample with progressive annealing duration t at 1673 K.

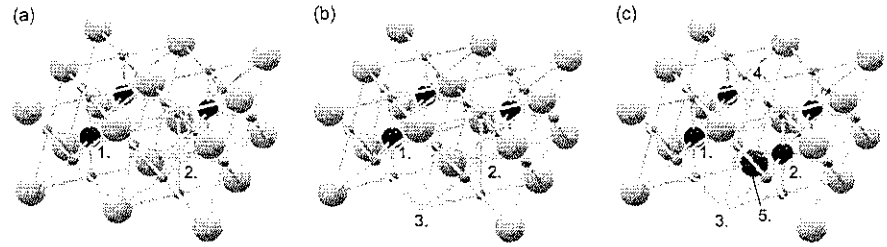

Fig. 7 Possible Ti motion in the $SrTiO_3$ lattice. The proportions of the different ionic species are for illustration purposes only and do not correspond to actual ionic radii. Black spheres: Ti; big grey spheres: Sr; small grey spheres: O. (a) The migration of the Ti ion (1) to the Ti vacancy (2) is energetically costly because of the O ion in between. (b) If an adjacent Sr vacancy is present (3), the Ti ion may reach (2) *via* (3). (c) If there is a second Sr vacancy in the vicinity (4), for example due to association with a La ion (5), the two Ti ions in (1) and (2) may change sites without needing an initial Ti vacancy.

includes the determination of the resolution function $R(x)$ and a deconvolution of depth profile data and $R(x)$ is quite complex (see, for example[33] and references therein). $R(x)$ can be approximated by a Gaussian function. The corresponding σ can in our case be estimated from the apparent width of the carbon layer by differentiation of the intensity data. The obtained values range between 0.7 and 2.4 nm, which is neglectably small compared to the σ values in Table 2. As eqn. 6 contains squared σ values, $R(x)$ becomes even less significant with increasing $\sigma_{post}/\sigma_{pre}$, because in this case D is determined predominantly by σ_{post}. Therefore, no $R(x)$ correction was applied.

Fig. 5 displays the diffusivities listed in Table 2 plotted against the annealing time. In spite of the large error of the first measurements, where the change in σ was only small, a slight time dependency of the diffusivities can not be excluded. A slight initial increase in the diffusivity due to chemical diffusion is expected, because after the implantation the Ti concentration at the maximum is 23.5 at% compared to 20 at% in the undisturbed crystal. Therefore, only the diffusion coefficients for $t_{tot} > 100$ h for 1573 K and $t_{tot} > 20$ h for 1673 K, respectively, were used for an Arrhenius fit, which leads to the following pre-exponential factor and activation enthalpy for 1 at% La-doped $SrTiO_3$:

$$D^{Ti}(1\,\text{at.\%La}) = 9.8 \times 10^{-11}\,\text{m}^2\,\text{s}^{-1} \exp\left(-\frac{321\,\text{kJ mol}^{-1}}{RT}\right) \quad \text{for } 1573\,\text{K} \leq T \leq 1673\,\text{K} \quad (9)$$

The corresponding value for the activation enthalpy per atom amounts to 3.3 eV. As the experiments were carried out at only two temperatures in a fairly narrow temperature range, this value has to be used with caution.

In contrast to 1 at% La-doped $SrTiO_3$, the 0.02 at% La-doped and undoped samples do not show significant diffusion after annealing times of up to 78 days at 1573 K and 42 days at 1673 K, respectively (see Fig. 6, Table 1). Hence, taking into account the analytical reproducibility, the diffusion coefficients must be lower than 1.4×10^{-23} m^2 s^{-1} at 1573 K, and 2.5×10^{-23} m^2 s^{-1} at 1673 K, respectively.

Compared to the La diffusion coefficients measured in,[26] Ti diffusion in the 1 at% La-doped crystals is about 2 orders of magnitude slower. This is not surprising, since the La and V''_{Sr} diffusion are connected,[26] and the calculated activation energy of V'''_{Ti} formation is much higher (11.59 eV) compared to V''_{Sr} (2.52 eV).[9] But whereas the values of D^{La} differ only by a factor of about 5 between undoped and 1 at% doped crystals, the dopant concentration dependence is much stronger in the case of Ti, where a factor of at least 100 is observed. Two explanations are possible:

1. A substantial amount of Ti vacancies is already present at 1 at% La-doping. Small amounts of Ti vacancies were however found only at [La] > 8 at%.[8] Also the big difference in the vacancy formation energies calculated by Akhtar *et al.* (see above) argues against this.

2. Ti migrates *via* Sr vacancies. Because of the high packing density interstitial sites do practically not exist in the $SrTiO_3$ lattice. Additionally, individual Ti ions are separated by oxygen ions and the anion sublattice is filled almost completely at oxidizing conditions. Therefore, the movement of the Ti ions from one Ti site to another may be considerably accelerated by hopping *via* Sr vacancies. In the case of association of two Sr vacancies, for example around a dopant ion, in principle no Ti vacancy is needed for the site change of two neighbouring Ti ions (see Fig. 7). Molecular dynamics studies addressing this point quantitatively would be quite interesting.

Lastly, a comparison with the earlier published diffusion data is difficult. Rhodes and Kingery give only the activation energy of 4.9 eV for Ti dislocation diffusion in undoped $SrTiO_3$ and a combined volume and pipe Ti diffusion coefficient of 7.8×10^{-22} m^2 s^{-1} at 2148 K in the same material.[25] Nevertheless these values and also the activation energy of 11.59 eV calculated by Akhtar *et al.* (see above) are at least not contradictory to our data.

Acknowledgements

We want to thank Mr F. Jomard for performing some of the SIMS analyses and Dr B. Lesage for making those SIMS analyses possible. Financial support of the Deutsche Forschungsgemeinschaft (DFG) is gratefully acknowledged.

References

1 Y.-M. Chiang, D. P. Birnie III and W. D. Kingery, *Physical Ceramics. Principles for Ceramic Science and Engineering*, Wiley, New York, 1997, p. 225–233.
2 R. Moos and K. H. Härdtl, *J. Am. Ceram. Soc.*, 1997, **80**, 2549.
3 F. A. Kröger and H. J. Vink, *Solid State Phys.*, 1956, **3**, 307.
4 U. Balachandran and N. G. Eror, *J. Mater. Sci.*, 1982, **17**, 2133.
5 U. Balachandran and N. G. Eror, *J. Electrochem. Soc.*, 1982, **129**, 1021.
6 W. Menesklou, *Fortsch. Ber. VDI, Reihe 5*, 1997, **481**.
7 T. Y. Tien and F. A. Hummel, *Trans. Br. Ceram. Soc.*, 1967, **66**, 233.
8 R. Moos, T. Bischoff, W. Menesklou and K. H. Härdtl, *J. Mater. Sci.*, 1997, **32**, 4247.
9 M. J. Akhtar, Z.-U.-N. Akhtar, R. A. Jackson and C. R. A. Catlow, *J. Am. Ceram. Soc.*, 1995, **78**, 421.
10 K. Wright and G. D. Price, *J. Geophys. Res.*, 1993, **98**, 22245.
11 S. N. Ruddlesden and P. Popper, *Acta Crystallogr.*, 1958, **11**, 54.
12 W. Menesklou, H.-J. Schreiner, K. H. Härdtl and E. Ivers-Tiffée, *Sens. Actuators B*, 1999, **59**, 184.
13 M. A. McCoy, R. W. Grimes and W. E. Lee, *Philos. Mag. A*, 1997, **75**, 833.

14 R. Meyer, R. Waser, J. Helmbold and G. Borchardt, *Phys. Rev. Lett.*, 2003, **90**, 105 901.
15 R. Meyer, R. Waser, J. Helmbold and G. Borchardt, *J. Electroceram.*, 2002, **9**, 101.
16 K. Szot, W. Speier, U. Breuer, R. Meyer, J. Szade and R. Waser, *Surf. Sci.*, 2000, **460**, 112.
17 Han Wei, W. Maus-Friedrichs, G. Lilienkamp, V. Kempter, J. Helmbold, K. Gömann and G. Borchardt, *J. Electroceram.*, 2002, **8**, 221.
18 A. Gunhold, K. Gömann, L. Beuermann, M. Frerichs, G. Borchardt, V. Kempter and W. Maus-Friedrichs, *Surf. Sci.*, 2002, **507–510**, 447.
19 R. Meyer, K. Szot and R. Waser, *Ferroelectrics*, 1999, **224**, 751.
20 K. Szot and W. Speier, *Phys. Rev. B*, 1999, **60**, 5909.
21 A. Gunhold, L. Beuermann, M. Frerichs, V. Kempter, K. Gömann, G. Borchardt and W. Maus-Friedrichs, *Surf. Sci.*, 2003, **523**, 80.
22 A. Gunhold, K. Gömann, L. Beuermann, G. Borchardt, V. Kempter and W. Maus-Friedrichs, *Anal. Bioanal. Chem.*, 2003, **375**, 924.
23 J. Helmbold, PhD Thesis, Technische Universität Clausthal, Germany, 2001.
24 F. Poignant and P. Abélard, *Key Eng. Mater.*, 1997, **132–136**, 1337.
25 W. H. Rhodes and W. D. Kingery, *J. Am. Ceram. Soc.*, 1966, **49**, 521.
26 K. Gömann, G. Borchardt, A. Gunhold, W. Maus-Friedrichs, B. Lesage, O. Kaïtasov and H. Baumann, *Mater. Res. Soc. Proc.*, 2003, **756**, EE3.1.1.
27 A. Gunhold, L. Beuermann, K. Gömann, G. Borchardt, V. Kempter, W. Maus-Friedrichs, S. Piskunov, E. A. Kotomin and S. Dorfman, *Surf. Interface Anal.*, 2003, **35**, 998.
28 A. Gunhold, K. Gömann, L. Beuermann, G. Borchardt, V. Kempter and W. Maus-Friedrichs, *Surf. Sci.*, in print.
29 H. Ryssel and I. Ruge, *Ion Implantation*, Wiley, Chichester, 1986, p. 14.
30 H. Heinrichs and A. G. Herrmann, *Praktikum der Analytischen Geochemie*, Springer, Berlin, 1990, p. 112.
31 *Sputtering by Particle Bombardment II: Sputtering of Alloys and Compounds, Electron and Neutron Sputtering, Surface Topography*, ed. R. Behrisch, Topics in Applied Physics, Springer, Berlin, 1983, vol. 52.
32 http://www.srim.org/; see also J. F. Ziegler, H. Biersack and U. Littmark, *The Stopping and Range of Ions in Solids*, Pergamon, Oxford, 1985, p. 202–262.
33 P. Fielitz, G. Borchardt, M. Schmückerand and H. Schneider, *Phys. Chem. Chem. Phys.*, 2003, **5**, 2279.

